

 Open access • Journal Article • DOI:10.1088/0964-1726/24/11/115037

Multimodal vibration damping of a beam with a periodic array of piezoelectric patches connected to a passive electrical network — [Source link](#)





Boris Lossouarn, Jean-François Deū, Mathieu Aucejo

Published on: 22 Oct 2015 - Smart Materials and Structures (IOP Publishing)

Topics: Vibration, Electrical network and Vibration control

Related papers:

- [Damping of structural vibrations with piezoelectric materials and passive electrical networks](#)
- [Broadband vibration control through periodic arrays of resonant shunts: experimental investigation on plates](#)
- [Multimodal passive vibration suppression with piezoelectric materials and resonant shunts](#)
- [Performance of piezoelectric shunts for vibration reduction](#)
- [Multimode vibration control using several piezoelectric transducers shunted with a multiterminal network](#)

Share this paper:    

View more about this paper here: <https://typeset.io/papers/multimodal-vibration-damping-of-a-beam-with-a-periodic-array-jpanoiapbl>



HAL
open science

Multimodal vibration damping of a beam with a periodic array of piezoelectric patches connected to a passive electrical network

Boris Lossouarn, Jean-François Deü, Mathieu Aucejo

► **To cite this version:**

Boris Lossouarn, Jean-François Deü, Mathieu Aucejo. Multimodal vibration damping of a beam with a periodic array of piezoelectric patches connected to a passive electrical network. *Smart Materials and Structures*, IOP Publishing, 2015, 24 (11), 10.1088/0964-1726/24/11/115037. hal-01691081

HAL Id: hal-01691081

<https://hal.archives-ouvertes.fr/hal-01691081>

Submitted on 22 Mar 2018

HAL is a multi-disciplinary open access archive for the deposit and dissemination of scientific research documents, whether they are published or not. The documents may come from teaching and research institutions in France or abroad, or from public or private research centers.

L'archive ouverte pluridisciplinaire **HAL**, est destinée au dépôt et à la diffusion de documents scientifiques de niveau recherche, publiés ou non, émanant des établissements d'enseignement et de recherche français ou étrangers, des laboratoires publics ou privés.

Multimodal vibration damping of a beam with a periodic array of piezoelectric patches connected to a passive electrical network

B Lossouarn ¹, J-F Deü ¹, M Aucejo ¹

¹ Structural Mechanics and Coupled Systems Laboratory, Conservatoire National des Arts et Métiers, 2 Rue Conté, 75003, Paris, France

E-mail: boris.lossouarn@cnam.fr

Abstract. A multimodal damping strategy is implemented by coupling a beam to its analogue electrical network. This network comes from the direct electromechanical analogy applied to a transverse lattice of point masses that represents the discrete model of a beam. The mechanical and electrical structures are connected together through an array of piezoelectric patches. A discrete and a semi-continuous model are proposed to describe the piezoelectric coupling. Both are based on the transfer matrix formulation and consider a finite number of patches. It is shown that a simple coupling condition gives a network that approximates the modal properties of the beam. A multimodal tuned mass effect is then obtained and a wide-band damping is introduced by choosing a suitable positioning for resistors in the network. The strategy and the models are experimentally validated by coupling a free-free beam to a completely passive network. A multimodal vibration reduction is observed, which proves the efficiency of the control solution and its potential in term of practical implementation.

PACS numbers: 85.50.-n, 63.10.+a, 46.40.Ff, 84.32.-y, 46.70.De

Keywords: vibration control, multimodal coupling, lattices, passive damping, piezoelectricity, shunt, electrical network

Submitted to: *Smart Mater. Struct.*

1. Introduction

A passive damping strategy was presented by Hagood and von Flotow [1] who proposed the use of piezoelectric material shunted with electrical circuits. The mechanical energy is converted in electrical energy before being dissipated into suitable resistors. Adding an inductor creates a resonant circuit that is the analogue of the tuned mass damper described by Den Hartog [2]. This significantly enhances the vibration reduction performances when the electrical resonance is tuned to the mechanical natural frequency to be controlled. When focusing on beam models, this effect can be described analytically [3, 4] but a finite element procedure [5] is often required for more complex structures. The concept of the piezoelectric damping was extended to the synthesis of metamaterials when came the idea of distributing a periodic array of shunted piezoelectric patches all over a mechanical structure. Considering one-dimensional media, longitudinal wave propagation was firstly analyzed [6, 7] and the strategy was then applied to bending waves control [8, 9, 10]. The classical passive resonant shunts can even be replaced by more broadband active solutions, as amplified resonant shunts [11] or negative capacitance shunts [12, 13]. The periodicity of the one-dimensional structures enables the use of the transfer matrix formulation, as proposed by Mead [14] who also gave results about the propagation constants. Structural discontinuities induces band gaps that can eventually be combined to the ones introduced by the piezoelectric shunts [6, 7, 9, 10, 11, 13].

As presented in the previous references, the strategy benefiting from the mechanical band gaps introduced by the addition of piezoelectric patches is limited to wavelength sufficiently small compared to the length of the patches. Consequently, it does not apply to the control of the first modes of the considered periodic structures. Moreover, an identical tuning of resonant shunts leads to a control only around a single frequency and still, high values of inductance are often required, which forces the use of non-passive synthetic inductors [8, 9, 10]. It is yet possible to reduce the required inductance by implementing a real electrical network connecting successive patches together. This strategy was firstly described by Valis et al. [15] who analyzed the coupling between traveling waves in a second-order electrical transmission line and

bending waves in a beam. The network consists of a line of inductors connected to the ground through the piezoelectric capacitance as it was also presented by Vidoli and dell'Isola [16]. It is observed that a mechanical damping can be achieved by introducing resistors and by tuning an electrical resonance to a target frequency [17]. However, even if the network has several resonances, the second-order architecture is efficient only for a single mode damping. A multimodal damping thus requires the implementation of fourth-order networks as those presented by Maurini et al. [18] and Bisegna et al. [19]. A limit is that the proposed networks includes negative inductors that can not be passive components. A solution for a passive multimodal control can be to numerically determine a network that matches a specified number of modes to control, along with a constraint based on use of only inductors and capacitors [20]. Yet, when considering a high number of mechanical modes, this solution leads to a network with an impractical number of electrical components. A suitable passive electrical architecture including transformers was given by Porfiri et al. [21, 22]. As it was shown that a multimodal control can be achieved with a network approximating the beam modal properties, the electrical topology is obtained from an electromechanical analogy [23, 24, 25]. This analogy, performed by Brillouin [26] on longitudinal periodic lattices, was already used to implement a multimodal control for longitudinal wave propagation [27]. The damping strategy is here extended to a bending wave control, which is modeled under a transfer matrix formulation based on electromechanical state vectors [28].

The transfer matrix formulation is firstly presented for a beam and for its equivalent transverse lattice obtained from a finite difference procedure. The direct electromechanical analogy is applied to this lattice in order to find the analogue electrical network of a beam. Both mechanical and electrical structures are then coupled through an array of piezoelectric patches. The analysis of the coupling is given by a linear model focusing on the global properties of a single unit cell, which represents a period of the structure. We propose a novel transfer matrix description of the coupled problem based on the discretization of the mechanical medium and a purely electrical representation. Afterwards, a more accurate semi-continuous model is presented to take into account the coupling of a continuous beam to its discrete analogue. Both models allows con-

sidering real applications where the number of patches remains limited. A multimodal coupling condition is given with original observations related to the introduction of damping elements. At the end, the damping strategy is experimentally validated with a passive network consisting of inductors and transformers. A method is also proposed to verify the tuning of the network from purely electrical measurements. All of this shows the potential of the strategy in terms of multimodal vibration reduction and proves its practical feasibility.

2. Wave propagation in a discretized beam

Wave propagation in a one-dimensional structure can be analyzed through the transfer matrix formulation. This applies to beams with a transfer matrix that is obtained from the Euler-Bernoulli theory. It is then remarked that a beam can be discretized into a periodic lattice model that approximates the continuous dispersion relation. The corresponding mechanical unit cell is presented together with its electrical analogue.

2.1. Transfer matrix formulation

A one-dimensional periodic structure is a series of identical unit cells [14]. For each unit cell, the relation between the mechanical states at its right and left ends can be described by a transfer matrix \mathbf{T} as

$$\begin{bmatrix} \mathbf{q}_R \\ \mathbf{F}_R \end{bmatrix} = \mathbf{T} \begin{bmatrix} \mathbf{q}_L \\ \mathbf{F}_L \end{bmatrix}, \quad (1)$$

where \mathbf{q}_L and \mathbf{q}_R are the displacements of the left and right ends of the unit cell. \mathbf{F}_R is the force applied on the considered cell by its right neighbor and \mathbf{F}_L is the force applied by the considered unit cell on its left neighbor. \mathbf{F}_L is thus defined as the opposite of the external force acting on the left end. This sign convention leads to the continuity of the state vector.

According to the definition of a periodic structure, each unit cell is described by an identical transfer matrix \mathbf{T} . Consequently, the mechanical state on the right of the n^{th} unit cell is obtained by raising \mathbf{T} to the power of n ,

$$\begin{bmatrix} \mathbf{q}_n \\ \mathbf{F}_n \end{bmatrix} = \mathbf{T}^n \begin{bmatrix} \mathbf{q}_0 \\ \mathbf{F}_0 \end{bmatrix} = \begin{bmatrix} \mathbf{T}_n^{qq} & \mathbf{T}_n^{qF} \\ \mathbf{T}_n^{Fq} & \mathbf{T}_n^{FF} \end{bmatrix} \begin{bmatrix} \mathbf{q}_0 \\ \mathbf{F}_0 \end{bmatrix}, \quad (2)$$

where the subscript 0 refers to the left end of the first unit cell. Then, when considering a finite number of n unit cells, the boundary conditions need to be introduced. For example, with a prescribed force \mathbf{F}_0 on the left end of a free-free periodic structure, as $\mathbf{F}_n = 0$, the displacement \mathbf{q}_n at the right end is defined by

$$\mathbf{q}_n = (\mathbf{T}_n^{qF} - \mathbf{T}_n^{qq}\mathbf{T}_n^{Fq}{}^{-1}\mathbf{T}_n^{FF})\mathbf{F}_0. \quad (3)$$

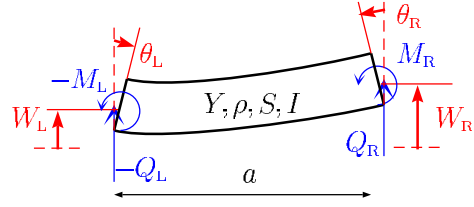


Figure 1. Considered beam segment.

2.2. Mechanical analysis of a beam

Wave propagation in a beam can be described by the Euler-Bernoulli theory, which considers small deflections, no shear strain and no rotational inertia. If Y is the Young's modulus of the beam, ρ its density, S its cross-section area and I its second moment of area, a bending wave equation is obtained when there is no distributed load,

$$\rho S \frac{\partial^2 w(x,t)}{\partial t^2} = -YI \frac{\partial^4 w(x,t)}{\partial x^4} \quad (4)$$

where $w(x,t)$ represents the transverse displacement at longitudinal location x and time t . A space-time separation $w(x,t) = W(x)g(t)$ applied on the wave equation (4) gives the general displacement amplitude solution under harmonic excitation

$$W(x) = A \cos(kx) + B \sin(kx) + C \cosh(kx) + D \sinh(kx) \quad (5)$$

and the corresponding dispersion relation

$$\omega^2 = \frac{YI}{\rho S} k^4, \quad (6)$$

where ω is the angular frequency and k is the wavenumber. The constants A , B , C and D depends on the boundary conditions, which are represented in figure 1 for a beam segment of length a . According to the Euler-Bernoulli beam theory, the transverse displacement $W(x)$, the rotation of the cross-section $\theta(x)$, the bending moment $M(x)$ and the shear force $Q(x)$ are governed by the equations

$$\begin{aligned} \theta(x) &= W'(x) \\ M(x) &= YI\theta'(x) \\ Q(x) &= -M'(x) \\ -\rho S \omega^2 W(x) &= Q'(x) \end{aligned}, \quad (7)$$

where $[\cdot]'$ represents the first space derivative. Consequently, it becomes possible to determine the constants appearing in (5) as

$$\begin{aligned} A &= \frac{1}{2}(W_L - \frac{1}{YIk^2}M_L) \\ B &= \frac{1}{2}(\frac{1}{k}\theta_L + \frac{1}{YIk^3}Q_L) \\ C &= \frac{1}{2}(W_L + \frac{1}{YIk^2}M_L) \\ D &= \frac{1}{2}(\frac{1}{k}\theta_L - \frac{1}{YIk^3}Q_L) \end{aligned}, \quad (8)$$

where the subscript L refers to the position $x = 0$. It can be noticed that the angle θ_L shows a negative value in figure 1, as it is represented in a clockwise direction. Finally, from (5), (7) and (8) for $x = a$, the expression

of the right state variables W_R , θ_R , M_R , and Q_R gives four equations that can be rearranged into matrix form as

$$\begin{bmatrix} W_R^* \\ \theta_R^* \\ M_R^* \\ Q_R^* \end{bmatrix} = \begin{bmatrix} \frac{c+\text{ch}}{2} & \frac{1}{ka} \frac{s+\text{sh}}{2} & -\frac{1}{(ka)^2} \frac{c-\text{ch}}{2} & \frac{1}{(ka)^3} \frac{s-\text{sh}}{2} \\ -ka \frac{s-\text{sh}}{2} & \frac{c+\text{ch}}{2} & \frac{1}{ka} \frac{s+\text{sh}}{2} & \frac{1}{(ka)^2} \frac{c-\text{ch}}{2} \\ -(ka)^2 \frac{c-\text{ch}}{2} & -ka \frac{s-\text{sh}}{2} & \frac{c+\text{ch}}{2} & -\frac{1}{ka} \frac{s+\text{sh}}{2} \\ -(ka)^3 \frac{s+\text{sh}}{2} & (ka)^2 \frac{c-\text{ch}}{2} & \frac{1}{ka} \frac{s-\text{sh}}{2} & \frac{c+\text{ch}}{2} \end{bmatrix} \begin{bmatrix} W_L^* \\ \theta_L^* \\ M_L^* \\ Q_L^* \end{bmatrix}, \quad (9)$$

where $c = \cos(ka)$, $\text{ch} = \cosh(ka)$, $s = \sin(ka)$, $\text{sh} = \sinh(ka)$, $W^* = W/a$, $\theta^* = \theta$, $M^* = aM/(YI)$ and $Q^* = a^2Q/(YI)$.

The previous system of equations (9) corresponds to the transfer matrix formulation described in (1). The displacement state vector is $\mathbf{q} = [W^* \ \theta^*]^T$ and the force state vector is $\mathbf{F} = [M^* \ Q^*]^T$. Dimensionless state variables are here considered in order to simplify the matrix form and to improve its conditioning. It is then possible to compute the frequency response of a finite structure consisting of n unit cells. For instance, with a free-free beam of length $l = na$ excited at one end, the displacements at the other end comes directly from (3) after computing the transfer matrix presented in (9).

2.3. Lattice model

The analysis of a homogeneous beam does not require to split the structure into several unit cells as the analytic formulation can be directly obtained with a beam segment equal to the entire beam. However, when considering a non-homogeneous medium as the discrete model of a beam, the local layout of the unit cells differs from the one of the whole structure. The transfer matrix formulation becomes then helpful as it allows computing the global mechanical behavior from the analytic description of a single unit cell.

The discrete model of a beam can be obtained through a finite difference procedure combining forward, central and backward differences:

$$\begin{aligned} [\cdot]_L' &= \frac{[\cdot]_I - [\cdot]_L}{a/2} \\ [\cdot]_I' &= \frac{[\cdot]_R - [\cdot]_L}{a} \\ [\cdot]_R' &= \frac{[\cdot]_R - [\cdot]_I}{a/2} \end{aligned} \quad (10)$$

where the subscript I defines the center of the considered unit cell. By applying those finite differences to the system of equations (7), it is obtained the relations between the left, center and right state variables of a discretized beam unit cell as

$$\begin{aligned} \frac{a}{2} \theta_L &= W_I - W_L \\ \frac{a}{2} \theta_R &= W_R - W_I \\ M_I &= K_\theta (\theta_R - \theta_L) \\ \frac{a}{2} Q_L &= M_L - M_I \\ \frac{a}{2} Q_R &= M_I - M_R \\ -m\omega^2 W_I &= Q_R - Q_L \end{aligned} \quad (11)$$

where $m = \rho S a$ is the mass of the unit cell and $K_\theta = YI/a$ is its bending stiffness. It can be remarked

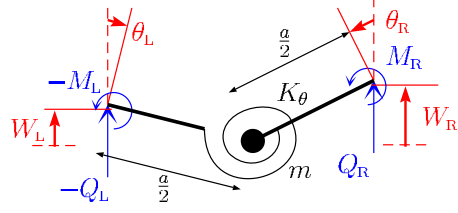


Figure 2. Discrete model of a beam segment.

that (11) defines a mechanical structure consisting of two massless rigid bars of length $a/2$ linked together through a pivot joint. At the pivot location are a lumped mass m and a torsion spring K_θ as represented in figure 2, which satisfy (11) for small displacements. W_I corresponds to the displacement of the mass m and M_I is the torque applied to the torsion spring K_θ . As a consequence, a beam can be approximated by a succession of identical unit cells referring to figure 2. This gives a lattice describing transverse wave propagation, which can be seen as an extension of the longitudinal spring mass lattice approximating wave propagation in a rod [25, 26, 27].

The equations (11) describing the mechanical behavior of the discrete unit cell are reorganized into a transfer matrix formulation as

$$\begin{bmatrix} W_R^* \\ \theta_R^* \\ M_R^* \\ Q_R^* \end{bmatrix} = \begin{bmatrix} 1 & 1 & \frac{1}{2} & -\frac{1}{4} \\ 0 & 1 & 1 & -\frac{1}{2} \\ \frac{f}{2} & \frac{f}{4} & 1 & -1 \\ -f & -\frac{f}{2} & 0 & 1 \end{bmatrix} \begin{bmatrix} W_L^* \\ \theta_L^* \\ M_L^* \\ Q_L^* \end{bmatrix}, \quad (12)$$

where $f = \omega^2 m a^2 / K_\theta$. The eigenvalues of a transfer matrix are related to the propagation constants of the corresponding one-dimensional problem [14]. For (12), two real and two complex eigenvalues are obtained that respectively refer to evanescent and propagative pairs of waves traveling in opposite directions. Considering the complex eigenvalues λ , they are related to \bar{k} , the equivalent wavenumber of the discrete problem, by $\lambda = \exp(\pm j \bar{k} a)$. So, it is found that $f = (2 \sin(\bar{k} a / 2))^4$, which gives the lattice dispersion relation when $\bar{k} a \leq \pi$

$$\omega^2 = \frac{YI}{\rho S} \left(\bar{k} \operatorname{sinc} \left(\frac{\bar{k} a}{2} \right) \right)^4. \quad (13)$$

By comparing this equation to the beam dispersion relation (6), it is seen that they are equivalent when $\bar{k} a$ goes to zero. This condition occurs when the length of the unit cell is sufficiently small compared to the considered wavelength. As a reference, it can be seen from (13) that 10 unit cells per wavelength ($\bar{k} a = 2\pi/10$) gives a frequency for the discrete model 3.25% lower than the frequency obtained with the continuous beam dispersion relation. This decrease of frequency is due to the fact that the discrete unit cell overestimates the kinetic energy of a continuous beam segment. As a conclusion, it is shown that a beam

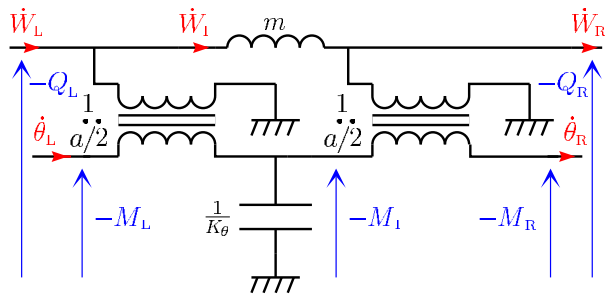


Figure 3. Electrical analogue of the discrete beam segment.

can be approximated by the lattice of point masses introduced in figure 2 as long as the number of unit cells per wavelength is sufficiently large to satisfy the desired frequency accuracy.

2.4. Direct electrical analogue

The system of equations (11) was firstly represented through the mechanical unit cell in figure 2 but it is also possible to define an analogue electrical representation. Using the direct electromechanical analogy [23, 24], a voltage is analogous to a force or a moment and a current is analogous to a linear or an angular velocity. As a consequence, a mass is represented by an inductance and a stiffness by the inverse of a capacitance.

When focusing on the unit cell presented in figure 2, it also requires to find the electrical analogues for the two levers of length $a/2$. It can be seen from (11) that the length $a/2$ corresponds to the proportionality constant between the transverse velocity differences and the angular velocities of the two rigid bars. Moreover, $a/2$ is also the proportionality constant between the bending moment differences and the shear forces in the same bars. This is finally modeled by an electrical transformer, where the ratio $a/2$ of the voltages on both windings is the inverse of the respective ratio of the intensities. All of this is illustrated in figure 3 where conventional electrical notations are replaced by their analogues that refer to the mechanical unit cell in figure 2. It is seen that the electrical unit cell strictly satisfies the equations (11), \dot{W}_1 representing the current flowing through the inductor m and M_1 being the voltage across the capacitance $1/K_\theta$. It is remarked that the network could have been obtained directly from the equations (11). However, applying the electro-mechanical analogy on the mechanical unit cell in figure 2 make easier the determination of the network topology.

A periodic electrical network is then created by serially connecting identical electrical unit cells. It is remarked that two transformers in a row can be

replaced by a single one with a doubled transformation ratio a . This is the equivalent of a rigid connection of two levers of length $a/2$, which gives a single lever of length a . Consequently, it is found a network architecture, which is similar to the one obtained by Porfiri et al. [21, 22] after a finite differentiation of the Timoshenko equations followed by a network simplification with the Euler-Bernoulli assumptions. At the end, it becomes possible to implement an electrical network that approximates the modal behavior of a beam. The electrical connections at both ends depend on the chosen mechanical boundary conditions. For example, referring to the direct electromechanical analogy, the analogue of a clamped beam would require open electrical connections. Indeed, a zero-current is analogous to a zero-velocity. However, a free-free beam requires grounded electrical connections at both ends, as a zero-voltage is analogous to a zero-force. Then, the network being constituted of discrete electrical components, it still refers to the transfer matrix (12) and the lattice dispersion relation (13). Electrical frequency responses can thus be computed with the same transfer matrix method as the one presented for the beam and its approximate discrete model.

3. Vibration control with a piezoelectric network

A multimodal vibration reduction of a beam can be achieved by the coupling to an electrical network approximating the modal properties of the beam. This is performed through a periodic distribution of piezoelectric patches. Discrete and semi-continuous models are proposed, both keeping the discrete nature of the network but considering the beam either as a lattice or as a continuous medium. The tuning of the network is then defined with a modal coupling condition and the choice of damping elements.

3.1. Global piezoelectric coupling

A homogeneous beam covered with a periodic distribution of piezoelectric patches is defined as a periodic structure. It is thus possible to extract the unit cell that repeats all along the structure. The considered unit cell is represented in figure 4 with a beam segment of length a , width b and thickness h_s . This unit cell is symmetrically covered with a pair of piezoelectric patches of length l_p , width b and thickness h_p . In order to control transverse vibrations, the patches are polarized in identical directions and electrically connected in parallel [1, 3, 18, 22].

As it is assumed that the piezoelectric patches are thin compared to the main structure ($h_p \ll h_s$), the bending motion of the beam mostly induces plane

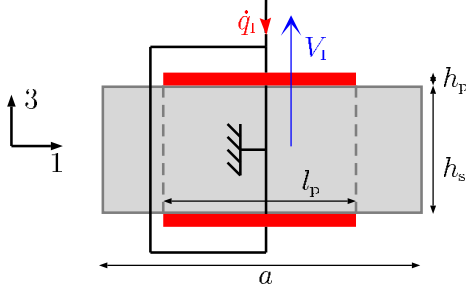


Figure 4. Beam segment with piezoelectric patches.

stress in the patches. Then, the 3D linear formulation can be simplified into the one-dimensional stress-charge form [5] of

$$\begin{aligned} \sigma_1 &= c_{11}^E \varepsilon_1 - \bar{e}_{31} E_3 \\ D_3 &= \bar{e}_{31} \varepsilon_1 + \bar{\epsilon}_{33}^E E_3 \end{aligned} \quad (14)$$

where '1' refers to the longitudinal direction and '3' to the direction of polarization. σ_1 and ε_1 thus represent the longitudinal stress and strain, D_3 and E_3 are the transverse electric displacement and electric field. For patches that are free along the '2' direction: $\bar{c}_{11}^E = 1/s_{11}^E$, $\bar{e}_{31} = d_{31}/s_{11}^E$ and $\bar{\epsilon}_{33}^E = \epsilon_{33}^E - d_{31}^2/s_{11}^E$, where s_{11}^E is the elastic compliance at constant electric field, d_{31} is the piezoelectric strain coefficient and ϵ_{33}^E is the permittivity at constant stress.

The longitudinal stress is seen as uniform along the cross-section and is given by $\sigma_1 = N_p/S_p$, N_p being the normal force into the patch and $S_p = bh_p$ its cross-section area. Still assuming a thin patch, the electric field E_3 is also considered as a constant [5]. E_3 is thus expressed from the voltage V_p between the two electrodes by $E_3 = -V_p/h_p$. At last, the electric charge q_p on an electrode of surface area $A_p = bl_p$ is related to the electric displacement by $q_p = -\int D_3 dA_p$. Consequently, the local piezoelectric formulation (14) can be recast into the global system

$$\begin{aligned} N_p &= Y_p^E S_p \varepsilon_1 - e_p V_p \\ q_p &= e_p \Delta U_p + C_p^\varepsilon V_p \end{aligned} \quad (15)$$

where ΔU_p is the difference between the longitudinal displacements at both ends of the piezoelectric patch, $Y_p^E = c_{11}^E$ is the short-circuited Young's modulus, $e_p = -b\bar{e}_{31}$ is the coupling coefficient and $C_p^\varepsilon = \bar{\epsilon}_{33}^E A_p/h_p$ the blocked capacitance.

As the longitudinal piezoelectric model (15) is obtained, it becomes possible to focus on the global electromechanical model of the unit cell presented in figure 4. In a first case, it is considered that patches cover the whole beam segment ($a = l_p$). We also make use of the fact that ε_1 can be approximated by $\Delta U_p/l_p$ for large wavelength compared to the unit cell. If $\Delta\theta = \theta_R - \theta_L$ represents the difference of the rotations

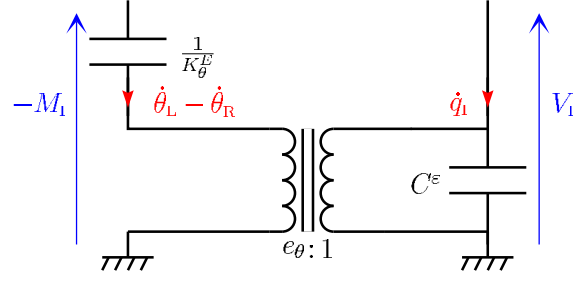


Figure 5. Electrical model of the piezoelectric coupling.

at both ends of the unit cell, $\Delta U_p = h_s \Delta\theta/2$. So, the bending model is obtained from (15) as

$$\begin{aligned} M_1 &= K_\theta^E \Delta\theta - e_\theta V_1 \\ q_1 &= e_\theta \Delta\theta + C^\varepsilon V_1 \end{aligned} \quad (16)$$

M_1 is the bending moment and K_θ^E is the bending stiffness when the pair of patches is short-circuited. K_θ^E is thus equal to $(Y_s I_s + 2Y_p^E I_p)/a$ where $I_s = bh_s^3/12$ and $I_p = b((h_s + 2h_p)^3 - h_s^3)/24$. The voltage V_1 and the charge q_1 are defined in figure 4, which gives $C^\varepsilon = 2C_p^\varepsilon$ and $e_\theta = h_s e_p$. The global formulation (16) can actually be illustrated by the electric scheme in figure 5. This model still use the direct electromechanical analogy, as it is the only analogy that allows the electrical representation of an energy conversion system based on the action of electrostatic forces [23]. The transformer represents the piezoelectric coupling as it links the mechanical branch on the left to the electrical branch on the right. This model comes directly from the one-dimensional linear piezoelectricity theory and is usually employed to describe a single piezoelectric patch [24]. It is here extended to the entire unit cell by focusing on its global properties.

Nevertheless, two limits appears in the previous formulation. First of all, it seems important to keep the possibility to consider a unit cell where the patches do not cover the entire beam segment ($a \neq l_p$), which occurs in most practical configurations. Secondly, the definition of the modified material constants \bar{c}_{11}^E , \bar{e}_{31} and $\bar{\epsilon}_{33}^E$ assumed a free stress state along the direction '2' of the patches. This does not represent any classical implementation as, when the patches are glued on a structure, it obviously acts along both directions '1' and '2'. This clearly affects the permittivity $\bar{\epsilon}_{33}^E$, which was used to determine the blocked capacitance C^ε . The analytic calculation of C^ε is not trivial as it requires to perform a three-dimensional analysis. This was presented by Maurini et al. [3], who proposed a correction of the equivalent material properties. It is here chosen to focus on a more practical solution that gives us the global properties defined in the coupled linear model (16). First, in a general case considering

also $a \neq l_p$, the global bending stiffness is obtained from figure 4 by

$$\frac{1}{K_\theta^E} = \frac{l_p}{Y_s I_s + 2Y_p^E I_p} + \frac{a - l_p}{Y_s I_s}, \quad (17)$$

Then, if K_θ^D refers to the bending stiffness in open circuit ($\dot{q}_1 = 0$), it can be seen from figure 5 that $K_\theta^D = K_\theta^E + e_\theta^2/C^\varepsilon$. In a similar manner, the free capacitance C^σ is obtained when no bending moment is applied to the unit cell ($M_1 = 0$), which gives $C^\sigma = C^\varepsilon + e_\theta^2/K_\theta^E$. The global coupling coefficient e_θ and the blocked capacitance C^ε are thus expressed from

$$\begin{aligned} e_\theta &= \sqrt{K_\theta^E \left(1 - \frac{K_\theta^E}{K_\theta^D}\right) C^\sigma} \\ C^\varepsilon &= C^\sigma \frac{K_\theta^E}{K_\theta^D} \end{aligned} \quad (18)$$

The short-circuit bending stiffness K_θ^E is already known but it still remains to define the open-circuit bending stiffness K_θ^D and the free capacitance C^σ . K_θ^D is directly obtained from (17) by replacing the piezoelectric Young's modulus in short-circuit Y_p^E by $Y_p^D = 1/(s_{11}^E - d_{31}^2/\epsilon_{33}^\sigma)$, that represents the equivalent Young's modulus in open-circuit. Concerning the capacitance, it still requires a three dimensional calculation but it can also be directly measured on the patches. This electrical measurement is actually not an easy task with C^ε as it would be required to mechanically block the ends of the unit cell. That is the reason why we focus on C^σ , which offer an easier measurement based on free mechanical boundary conditions. The global bending model for a piezoelectrically coupled unit cell is thus finally obtained by following the same method as was described in [27] for a longitudinal case.

3.2. Discrete electromechanical model

In the present section, our main goal is to model and observe the behavior of a continuous structure that is coupled to a network of electrical components through a periodic distribution of piezoelectric patches. As presented by Vidoli and dell'Isola [16] and Maurini et al. [18], a wide-band energy exchange can be achieved by connecting a mechanical structure to its electrical analogue. The coupling of a rod to a line of inductors was implemented in a previous paper [27]. This strategy is here extended to the case of a beam. So, the chosen network is the one represented by the unit cell in figure 3, as considered by Porfiri et al. [21, 22]. Because this network can approximate the dispersion relation of a beam, analogue boundary conditions gives similar modal properties. However, we deal with two structures of different natures: the beam is continuous and the network is discrete. In order to simplify the analysis, it is yet convenient to

set up an analytic model combining two structures of identical nature. This is the reason why most of the papers focusing on the piezoelectric coupling of a beam to an electrical network perform an homogenization of the electrical medium [15, 16, 18, 19, 20, 21, 22]. This homogenization is justified for a large number of piezoelectric elements. Nevertheless, when considering practical implementations, the number of components can be limited and the network needs to be modeled as a discrete structure. Consequently, another solution bringing together two structures of similar nature is to discretize the mechanical medium. The beam is approximated by its lattice model in figure 2, which can also be represented by the electrical scheme in figure 3. Therefore, the initial electromechanical problem can be reviewed into the interaction of two electrical networks having the same architecture.

The mechanical and the electrical unit cells are interacting through a piezoelectric coupling. This coupling is modeled by the electrical representation in figure 5. As a consequence, the electromechanical unit cell including a network segment is given in figure 6. As seen in section 2, the mass m involved in the mechanical lattice comes directly from the total mass of the continuous unit cell:

$$m = \rho_s S_s a + 2\rho_p S_p l_p, \quad (19)$$

where ρ_s and ρ_p are respectively the density of the main structure and the density of the piezoelectric patches and $S_s = bh_s$ is the cross-section area of a patch. Concerning the electrical part, the currents \dot{q}_w and \dot{q}_θ are the analogues of the velocities \dot{W} and $\dot{\theta}$ and the voltages V_θ and V_w are the analogues of the bending moment $-M$ and the shear force $-Q$, referring to figure 3. The network capacitance can be directly the blocked capacitance of pair of patches, C^ε , which avoid adding any complementary capacitors. Then, the network segment consists of two transformers of ratio $\hat{a}/2$ and an L inductor.

From the electrical equations governing figure 6, the 8 ports electromechanical unit cell can be described by the transfer matrix

$$\begin{bmatrix} W_\theta^* \\ \theta_\theta^* \\ q_w^* \\ q_\theta^* \\ M^* \\ Q^* \\ V_\theta^* \\ V_w^* \end{bmatrix} = \begin{bmatrix} 1 & 1 & 0 & 0 & \frac{1}{2} & -\frac{1}{4} & \frac{\Lambda}{2e_\theta} & -\frac{\Lambda}{4e_\theta} \\ 0 & 1 & 0 & 0 & 1 & -\frac{1}{2} & \frac{\Lambda}{e_\theta} & -\frac{\Lambda}{2e_\theta} \\ 0 & 0 & 1 & 1 & -\frac{e_\theta}{2} & \frac{e_\theta}{4} & -\frac{1+\Lambda}{2} & \frac{1+\Lambda}{2} \\ 0 & 0 & 0 & 1 & -e_\theta & \frac{e_\theta}{2} & -(1+\Lambda) & \frac{1+\Lambda}{2} \\ \frac{f}{2} & \frac{f}{4} & 0 & 0 & 1 & -1 & 0 & 0 \\ -f & -\frac{f}{2} & 0 & 0 & 0 & 1 & 0 & 0 \\ 0 & 0 & -\frac{f}{2} & -\frac{f}{4} & 0 & 0 & 1 & -1 \\ 0 & 0 & f & \frac{f}{2} & 0 & 0 & 0 & 1 \end{bmatrix} \begin{bmatrix} W_\theta^* \\ \theta_\theta^* \\ q_w^* \\ q_\theta^* \\ M^* \\ Q^* \\ V_\theta^* \\ V_w^* \end{bmatrix}, \quad (20)$$

where $f = \omega^2 m a^2 / K_\theta^E$, $\tilde{f} = \omega^2 L C^\varepsilon \hat{a}^2$ and $\Lambda = e_\theta^2 / (K_\theta^E C^\varepsilon)$. Nondimensionalization is performed as in (9) and (12), which transforms the state variables as follows: $W^* = W/a$, $\theta^* = \theta$, $M^* = M/K_\theta^E$, $Q^* = aQ/K_\theta^E$, $q_w^* = q_w/\hat{a}$, $q_\theta^* = q_\theta$, $V_\theta^* = C^\varepsilon V_\theta$, $V_w^* = \hat{a} C^\varepsilon V_w$. It becomes then possible to compute the behavior of a succession of several electromechanical

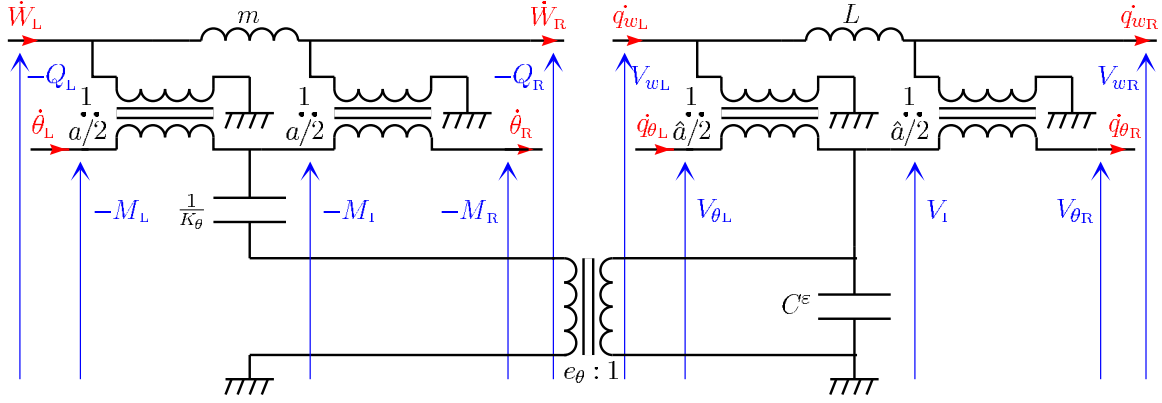


Figure 6. Electrical model of the coupling between the discrete beam segment and its analogue network.

unit cells from (2) with $\mathbf{q} = [W^* \ \theta^* \ q_w^* \ q_\theta^*]^T$ and $\mathbf{F} = [M^* \ Q^* \ V_\theta^* \ V_w^*]^T$.

3.3. Semi-continuous model

The discrete model was obtained by approximating the continuous beam segment presented in figure 1 by its lattice model described in figure 2. As mentioned in section 2, this approximation is only valid when the considered wavelength is large compared to the length of the unit cells. A classical limit can be 10 unit cells per wavelength, which allows a frequency error of less than 4% as given by (13). However, when the number of piezoelectric patches is limited, the discrete model becomes too inaccurate to describe the behavior of the mechanical structure. As highlighted by Bisegna et al. [19], it is thus essential to develop a semi-continuous model that maintains the continuity of the beam together with a discrete electrical network.

In order to keep the model as simple as possible, it is chosen to consider an homogeneous unit cell, without taking into account the discontinuity induced by the thickness of the patches. This does not significantly influence the results as the band gap phenomenon [6, 7, 9, 10, 11] only occurs when the wavelength approaches the length of the unit cell. Consequently, we keep the global constants appearing in (16) for a discrete model, but the continuity of the mechanical medium is recovered by replacing $\Delta\theta$ by $a\theta'(x)$ in the bending moment equation. The piezoelectric coupling on a continuous beam segment is then

$$\begin{aligned} M(x) &= Y^E I \theta'(x) - e_\theta V_1 \\ q_1 &= e_\theta \Delta\theta + C^\epsilon V_1 \end{aligned} \quad (21)$$

where $Y^E I = K_\theta^E a$. Then, we can consider a new state variable $M(x) + e_\theta V_1 = Y^E I \theta'(x)$ that does not depend on the electrical state anymore. This state variable thus represents the bending moment of a purely mechanical problem that can be written under

the form

$$\begin{bmatrix} W_R^* \\ \theta_R^* \\ M_R^* + \frac{\Delta}{e_\theta} V_1^* \\ Q_R^* \end{bmatrix} = \mathbf{T}_m \begin{bmatrix} W_L^* \\ \theta_L^* \\ M_L^* + \frac{\Delta}{e_\theta} V_1^* \\ Q_L^* \end{bmatrix}, \quad (22)$$

where \mathbf{T}_m is the transfer matrix in (9) with $k = \sqrt[4]{\rho S \omega^2 / Y^E I}$ and $\rho S = m/a$. Furthermore, the modeling of the electrical network being unchanged, the electrical state variable can still be described from figure 6, which gives

$$V_1^* = \begin{bmatrix} 0 \\ 0 \\ 1 \\ -\frac{1}{2} \end{bmatrix}^T \begin{bmatrix} q_{wL}^* \\ q_{\theta L}^* \\ V_{\theta L}^* \\ V_{wL}^* \end{bmatrix} = \begin{bmatrix} 0 \\ 0 \\ 1 \\ \frac{1}{2} \end{bmatrix}^T \begin{bmatrix} q_{wR}^* \\ q_{\theta R}^* \\ V_{\theta R}^* \\ V_{wR}^* \end{bmatrix} \quad (23)$$

and

$$\begin{bmatrix} q_{wR}^* \\ q_{\theta R}^* \\ V_{\theta R}^* \\ V_{wR}^* \end{bmatrix} = \mathbf{T}_e \begin{bmatrix} q_{wL}^* \\ q_{\theta L}^* \\ V_{\theta L}^* \\ V_{wL}^* \end{bmatrix} + e_\theta (\theta_L^* - \theta_R^*) \begin{bmatrix} \frac{1}{2} \\ 1 \\ 0 \\ 0 \end{bmatrix}, \quad (24)$$

where \mathbf{T}_e is the transfer matrix in (12) with f replaced by \tilde{f} . Combining equations (22), (23) and (24) leads to the matrix form

$$\begin{aligned} & \left[\begin{array}{cc} e_\theta \left[\begin{array}{cc} I_4 & \mathbf{o}_2 \\ \mathbf{o}_2 & \mathbf{o}_2 \end{array} \right] & \mathbf{o}_4 \\ \mathbf{o}_4 & I_4 \end{array} \right] \left[\begin{array}{c} I_4 \\ \frac{\Delta}{e_\theta} \left[\begin{array}{cc} \mathbf{o}_2 & \mathbf{o}_2 \\ \mathbf{o}_2 & I_4 \end{array} \right] \end{array} \right] \left[\begin{array}{c} W_R^* \\ \theta_R^* \\ M_R^* \\ Q_R^* \\ q_{wR}^* \\ q_{\theta R}^* \\ V_{\theta R}^* \\ V_{wR}^* \end{array} \right] \\ & = \left[\begin{array}{cc} \mathbf{T}_m & \frac{\Delta}{e_\theta} \mathbf{T}_m \left[\begin{array}{cc} \mathbf{o}_2 & \mathbf{o}_2 \\ \mathbf{o}_2 & \left[\begin{array}{cc} 1 & -\frac{1}{2} \\ 0 & 0 \end{array} \right] \end{array} \right] \\ e_\theta \left[\begin{array}{cc} \mathbf{o}_2 & \mathbf{o}_2 \\ \left[\begin{array}{cc} 0 & \frac{1}{2} \\ 0 & 1 \end{array} \right] & \mathbf{o}_2 \end{array} \right] & \mathbf{T}_e \end{array} \right] \left[\begin{array}{c} W_L^* \\ \theta_L^* \\ M_L^* \\ Q_L^* \\ q_{wL}^* \\ q_{\theta L}^* \\ V_{\theta L}^* \\ V_{wL}^* \end{array} \right], \end{aligned}$$

where \mathbf{I}_4 represents a 4×4 identity matrix, \mathbf{o}_4 is a 4×4 zero matrix and \mathbf{o}_2 a 2×2 zero matrix. At last, equation (25) can be rearranged into a transfer matrix giving the relation between the displacements, electric charges, forces and voltages at both ends of the unit cell.

3.4. Multimodal coupling

The main interest of the electrical network is that it can approximate the modal behavior of the mechanical structure to control. A modal coupling optimizing the energy transfer between the two media is obtained when they have a same dispersion relation and analogous boundary conditions [18]. The considered network being discrete, its electrical components are thus tuned to equal the dispersion relation related to the lattice model of the beam. When looking at the transfer matrix (12) defining the discrete mechanical unit cell in figure 2, it is remarked that another unit cell having a same architecture would present similar modal properties if it has a same ratio $K_\theta/(a^2m)$. Consequently, with analogous boundary conditions, a transverse lattice and its analogue electrical network exhibit the same natural frequencies and the same mode shapes if

$$\frac{1}{\hat{a}^2} \frac{1}{LC^\varepsilon} = \frac{1}{a^2} \frac{K_\theta^E}{m}. \quad (26)$$

With the analogue network and this coupling condition, the resonances do not only match along the frequency domain but also on the spatial domain thanks to similar mode shapes. Here is thus added an electrical space dimension, which does not appear with an array of passive resonant shunts that are independently tuned to a single natural frequency [6, 7, 9, 10].

Furthermore, the global capacitance of a unit cell C^ε is approximately proportional to A_p , the surface area of a piezoelectric patch. For a fixed thickness of the patches and fixed length and width of the beam, A_p is then proportional to $1/n$, where n is the number of unit cells. So, it is seen from the modal coupling condition (26) that a prescribed amount of piezoelectric material leads to $L \propto 1/n^3$. This result was also obtained by Maurini et al. [18] from the homogenized analysis of various fourth-order networks. An increase in the number of unit cells gives lower values of the required inductance. It becomes thus possible to consider low frequency applications without being limited by available values of passive inductors.

By applying the coupling condition (26) to a network that is piezoelectrically connected to a beam, one creates the equivalent of a multimodal tuned mass control [2]. As it was already obtained with a rod in [27], an antiresonance surrounded by two new resonances appears around the initial natural frequency. This effect is shown in figure 7 that represents the mobility frequency response function (FRF) for the transverse velocity at one end of a free-free beam and a shear force applied at the other end. The responses are computed for a one meter beam in aluminum alloy 2017, which is periodically covered with $n = 20$ pairs of PZT patches. The geometry and the material constants are presented

in table 1. The analysis of the free-free structure

Table 1. Geometry and material properties.

	Beam (Al 2017)	Patches (PZT)
Length	$l_s = Na = 20 \times 5$ cm	$l_p = 3$ cm
Width	$b = 2$ cm	$b = 2$ cm
Thickness	$h_s = 2$ cm	$h_p = 0.5$ mm
Density	$\rho_s = 2780$ kg/m ³	$\rho_p = 7800$ kg/m ³
Young's modulus	$Y_s = 73.9$ GPa	$1/s_{11}^E = 66.7$ GPa
Charge constant	-	$d_{31} = -210$ pC/N
Permittivity	-	$\epsilon_{33}^s = 21.2$ nF/m

consisting of 20 coupled unit cells is performed through the transfer matrix formulation (3), both with the discrete model (20) and the semi-continuous model (25). It is noticed that the same matrices would also be used for other boundary conditions. The global equation (3) is only valid for a free-free structure but equivalent formulations can be obtained from (2) for other boundary conditions. In any case, it is observed that the difference between the discrete model and the semi-continuous model increases with the frequency as the transverse lattice becomes more and more inaccurate for the approximation of the continuous beam. Still, depending on the application, the discrete model can be sufficient as long as the number of unit cells per wavelength is high enough. For example, the error is here observable around the fourth open-circuited mode, but it would have been insignificant with $n = 40$ unit cells. Also, with a limited number of unit cells, as the network is tuned to fit the modes of the transverse lattice, it does not match exactly the modes of the continuous beam. The mechanical antiresonances observed in figure 7 are related to the electrical resonances. It is seen that the mistuning increases with the frequency: the fourth antiresonance is clearly shifted to lower frequencies compared to the fourth open-circuited mechanical resonance. It is thus essential to determine the highest mode to be controlled before choosing the number of piezoelectric patches that will cover the mechanical structure. For an insufficient number of patches, the highest electrical resonances would not match the corresponding mechanical modes and the multimodal control performances could be considerably reduced.

3.5. Multimodal damping

A reduction of vibration on a wide frequency range requires the tuning of the inductors but also the introduction of suitable damping components. A classical solution presented in most papers focusing on piezoelectric shunts is to add resistors in series with the inductors [1, 4, 6, 7, 8, 10, 28]. Another less common solution consist in connecting resistors in

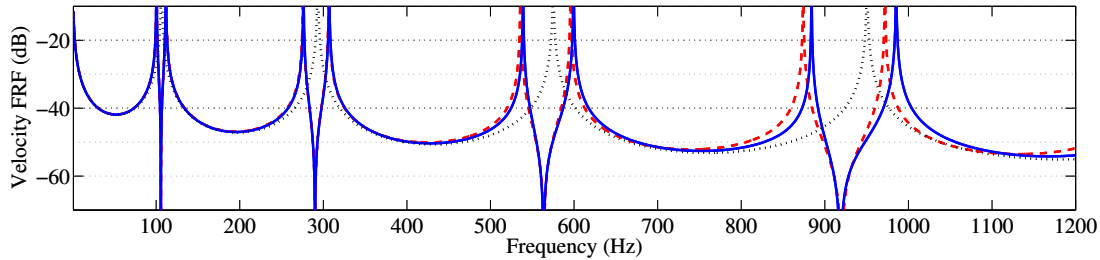


Figure 7. Velocity at the free end of the beam for a unit force applied at its exited end. - (···) semi-continuous model without network (open-circuit), (---) discrete model with a non-dissipative network satisfying the modal coupling condition, (—) semi-continuous model with a non-dissipative network satisfying the modal coupling condition.

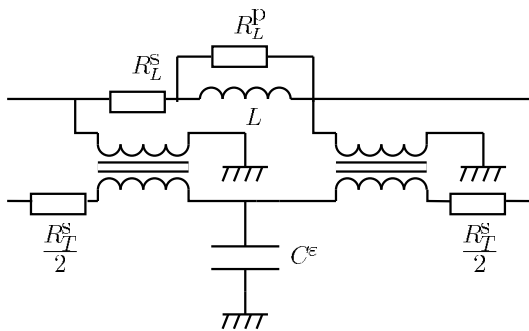


Figure 8. Network segment including resistors.

parallel with the inductors [17, 18, 19, 20]. It becomes then possible to tune the resistors in order to reach a vibration reduction optimum, which is here defined as a minimum amplitude on the velocity FRF. However, even if for both damping strategies an optimum can be reached at one particular frequency, there is no reasons to expect an optimal damping on a wide frequency range. Another damping model was proposed by Porfiri et al. [21] to get a multimodal damping with the analogue network of a beam. The solution is to add resistors R_T^S in series with the windings of the transformers. This is presented on the network segment in figure 8, which also shows R_L^S and R_L^D , the serial and parallel resistors connected to the inductors.

In figure 9, the three damping models are compared by computing the semi-continuous model with a transformer ratio $\hat{a} = 1$ and the effect of resistors added in (23) and (24). The free-free coupled beam previously described in table 1 is still the relevant case. The damping is considered optimal around one mode when the corresponding highest local maximum of the velocity FRF is reduced to its minimum value. We define as underdamped a mode where it can be seen a local minimum and overdamped thus corresponds to a case where there is no local minimum. Independently of the chosen damping model, the resistors are tuned to reach an optimum around the first initial mode

of the beam. With only a serial resistance in the inductors ($R_T^S = 0 \Omega$ and $R_L^D \rightarrow +\infty$), $R_L^S = 20 \Omega$ leads to the maximal vibration reduction around the first mode but it also gives a clear underdamped behavior for higher modes. On the other hand, with $R_L^D = 1000 \Omega$, $R_L^S = 0$ and $R_T^S = 0$, the first mode is still optimized but the other ones are overdamped. At last, when $R_L^D = 150 \Omega$, $R_L^S = 0$ and $R_L^D \rightarrow +\infty$, it appears a slightly underdamped behavior. It is thus observed that the damping involving resistors in the transformer windings leads to highest vibration reduction around each mode. Nevertheless, the damping is still only optimal for the first mode, while it could be expected from [21] an optimal damping for all the modes together. The first reason is that this last reference focus on an electrical continuum. The work here considers a discrete network, which cannot match exactly the modes of the continuous mechanical structure. This effect can be observed through the position of the local maxima for which the asymmetry increases with the frequency. The second reason explaining why the present damping with R_T^S is not optimal is related to the boundary conditions. It was mentioned in [21] that the proposed optimal damping is only valid with boundary conditions ensuring global solutions represented by trigonometric eigenfunctions. This is true for a simply supported beam but not for the considered case of a free-free beam. Finally, although not really optimal in a general case involving a finite number of patches and no trigonometric boundary conditions, the damping involving the resistance R_T^S remains a satisfactory sub-optimal solution compared to the other damping models. Depending on the choice of the electrical components, several damping elements can be combined together but a recommendation would be to keep R_T^S as the main dissipative component.

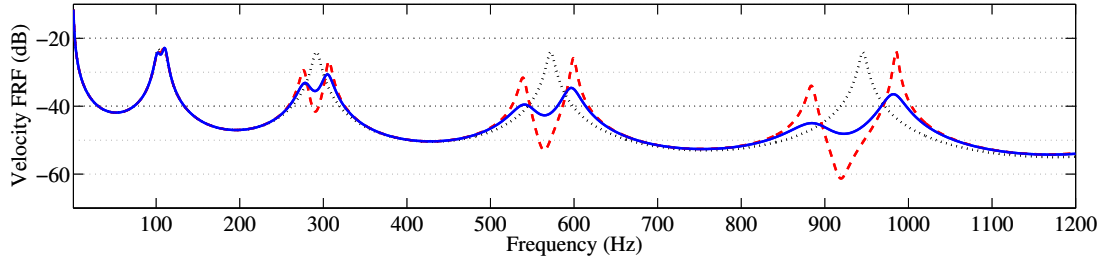


Figure 9. Velocity FRF computed with the semi-continuous model and a network satisfying the modal coupling condition. - (···) with a parallel resistance $R_L^P = 1000 \Omega$ on the inductors, (- -) with a serial resistance $R_L^S = 20 \Omega$ on the inductors, (—) with a serial resistance $R_T^S = 150 \Omega$ on the transformers.



Figure 11. Placement of the shaker and the vibrometer.

4. Experiments and discussion

The multimodal damping strategy is validated with a setup involving a one meter free-free beam. Piezoelectric patches are periodically distributed and connected to a network of passive components. The properties of the network are verified by measuring voltage frequency response functions. Once the network is tuned, a mechanical analysis shows the efficiency of the strategy for vibration reduction.

4.1. Experimental setup

The structure described in table 1 constitutes the setup used to validate the multimodal damping strategy. 20 pairs of piezoelectric patches are glued to a one meter beam in aluminum alloy 2017. The resulting structure is suspended by elastic straps in order to approximate free-free boundary conditions. Then, as presented in figures 10 and 11, a suspended shaker is transversely connected to one end of the beam through an impedance head that measures the acceleration and the transmitted force. A white noise excitation is generated from the shaker and the transverse

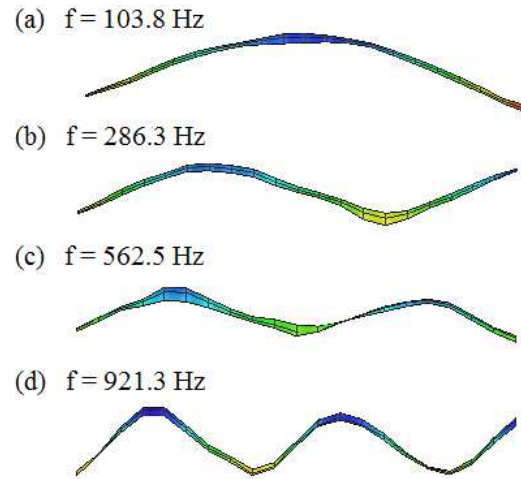


Figure 12. Mode shapes measured with the scanning vibrometer: (a) 1st mode, (b) 2nd mode, (c) 3rd mode, (d) 4th mode.

velocity of the beam is measured with a scanning laser vibrometer. To compute the velocity FRF, the force measured by the impedance head and the velocity at the free end of the beam are taken into account. The FRF is then obtained with a fast Fourier transform over a 1.2 kHz frequency range and a 0.2 Hz resolution.

The analysis is firstly performed without adding any electrical components on the piezoelectric patches. We focus on the first four modes that can be extracted thanks to a spatial scanning procedure that gives the results presented in figure 12. Afterwards, the experimental open-circuit FRF is compared to the results obtained with the purely mechanical homogenized model computed from (3) and (9). Concerning corrections of the model, the reduction of the piezoelectric Young's modulus determined from longitudinal experiments in [27] is maintained with the same multiplying coefficient $\gamma = 0.86$. Moreover, as the electrical connectors are part of the mechanical structure, there is a slight increase of the total moving



Figure 10. Experimental setup for the analysis of transverse waves.

mass. This effect is taken into account by multiplying the equivalent density by a coefficient $\beta = 1.03$, which is determined from the experimental FRFs. At the end, a mechanical damping model is required to approach the velocity maxima appearing when no control occurs. This global damping needs to model the internal dissipation in the structure but also the damping due to imperfect boundary conditions and the presence of the electrical connectors. It is seen that a viscous damping applied to the transverse displacement of the beam represents a suitable damping model for the first four modes. This is introduced by multiplying the density by a coefficient evaluated to $\alpha = 1 - 27j/\omega$ to fit the first four maxima.

4.2. Passive electrical network

After having validated the mechanical model of the beam, the multimodal network is implemented. It is chosen to create a completely passive solution without the use of any synthetic components. No capacitors are required because the capacitance C^ε involved in figure 6 is offered by the piezoelectric patches. Concerning the magnetic components, i.e. the inductors and the transformers, they were manufactured in order to obtain sufficiently low internal resistance. This was made possible by winding copper wire around ferrite cores presenting a closed magnetic circuit. The transformer windings connected to the patches had to be doubled to get around the fact that the pairs of patches were polarized in opposite direction, for practical reasons. In the present application, it was remarked that the transformers can be model as represented in figure 13, which takes only into account the element having a significant electrical influence on the considered 1.2 kHz frequency range. C_T is the capacitance between windings, L_T is the magnetizing inductance and R_T^S represents the copper losses in the windings. It was chosen to design transformers with a ratio $\hat{a} = 1$ and an internal resistance R_T^S around 150 Ω in order to approach the optimal damping determined in section 3, without adding external resistors. After manufacturing, direct measurements at 1 kHz gives $R_T^S = 153 \Omega$, $L_T = 12.1$ H and $C_T = 25.2$ nF. By introducing the parasitic elements in figure 6, it is remarked that C_T adds a parallel capacitance to C^ε . Consequently, the modal

coupling condition (26) needs to be computed with a global capacitance $C^\varepsilon + C_T$. C^ε being equal to 35.3 nF, it is obtained a target inductance value equal to 118 mH. The manufactured inductors are finally around $L = 121$ mH and their internal damping can be represented by a parallel resistance equal to 72 k Ω . The same type of parallel damping is also introduced for the capacitance, where the equivalent parallel resistance is evaluated to 332 k Ω at 1 kHz. A last step consists in verifying that $L \ll L_T$. Indeed, too much current leakage through the magnetizing inductance would modify the electrical modal properties that were designed from a model involving ideal transformers. Then, all the components are put together according to figure 6, which gives the network presented in figure 14, where the line of components on the bottom of the picture represents the inductors and the ones just above are the transformers.

The tuning of the electrical network can be verified before observing its effect on mechanical vibration

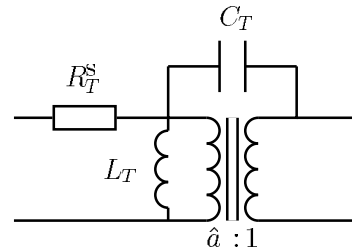


Figure 13. Electrical model for the transformers.

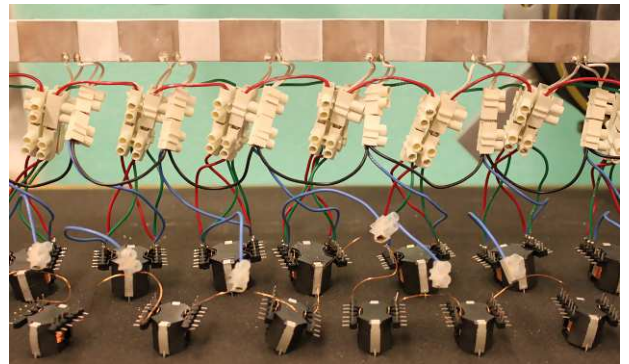


Figure 14. Electrical network involving inductors and transformers.

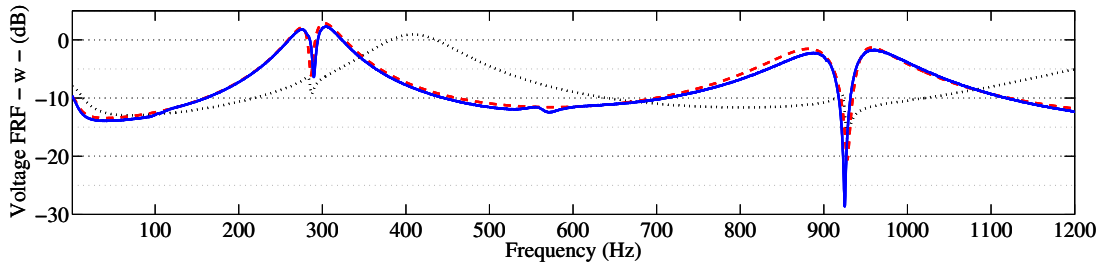


Figure 15. Electrical frequency response functions with measure of the voltage between the 10th and the 11th inductors - (\cdots) for the transfer matrix model with a detuned network, ($-\cdots$) for the transfer matrix model with a tuned network, ($-$) for the experiment with a tuned network.

reduction. A white noise voltage V_w is applied at one end and voltage is measured in the middle, between the 10th and the 11th inductors. The electrical frequency response function presented in figure 15 is obtained, with both the experimental result and the numerical computation based on the semi-continuous transfer matrix model (25). The analogue of this experiment in the mechanical domain would be to measure the shear force in the middle of the beam when applying a transverse force excitation at one end. With free-free boundary conditions, the middle of the beam is a node for the odd shear force modes. The same remark applies to the voltage in the inductor line as the electrical network was designed to tend to the analogue of the free-free beam. As a consequence, the measured voltage tracks only the even modes. The lowest resonance, around 290 Hz, is thus the second electrical resonance of the network and the one around 920 Hz is the fourth electrical resonance of the network. It is also seen sharp antiresonances that are an image of the mechanical resonances. Actually, part of the energy injected in the network flows to the coupled beam around the mechanical resonances, which creates cuts in the frequency spectrum. So, the tuning of the network is validated by verifying that the sharp antiresonances are centered on the smooth resonances. This is the case with the tuned electrical values but not for a detuned network with half of the required inductance, as it can be observed in figure 15.

With measurement of the voltage V_θ in the middle of the network, it is possible to extract the odd modes. This is explained by the fact that the middle of a free-free beam is a node for the even modes related to the bending moment, which is the analogue of V_θ . But the problem is that we do not have access to the measurement of the voltage V_θ in the middle of the network. This is because the two successive $\hat{a}/2$ transformers are replaced by a single \hat{a} transformers to limit the number of components. Nevertheless, it is still possible to observe the odd modes by measuring the voltage on one of the closest node, the 10th pair of piezoelectric patches. The results are represented

in figure 16 that also shows the case of a detuned network with half of the required inductance. As the measurement is not performed in the exact middle of the network, the even modes also appears. It is still possible to verify that the odd electrical resonances match the mechanical ones. As a consequence, the previous electrical FRFs allows being sure that the network is correctly tuned, even before doing any mechanical testing. The electrical FRFs also enable validating the presented transfer matrix formulation that takes into account the modeling of the electrical components. It is observed in figures 15 and 16 that the numerical and experimental curves are sufficiently close to validate the transfer matrix model. Thus, this model can be used to evaluate the vibration reduction depending on the choice of the electrical components.

4.3. Damping of bending modes

Once the electrical network is correctly tuned, it becomes possible to observe the effect of the multimodal coupling on the mechanical vibrations. In figure 17, the velocity FRF with a tuned network can be compared to the velocity FRF with open-circuited patches. Reductions are observed of around 7 dB for the first mode, 10 dB for the second and third modes and 16 dB for the fourth mode, which shows the efficiency of the present damping strategy involving a multimodal network. However, a velocity FRF similar to the one presented in figure 9 is not obtained. The system seems overdamped as no local minimum appears, even with the prescribed resistance R_T^S . This is due to the fact that the added winding capacitance C_T was clearly non-negligible compared to the piezoelectric capacitance C^ε , which was not expected before manufacturing the transformers. The final global capacitance of the unit cell was almost doubled and this led to a reduction of the required inductance. The transformer resistance having been defined without considering capacitance addition, it becomes too high for the present inductance. It is noticed that the capacitance C_T could have been

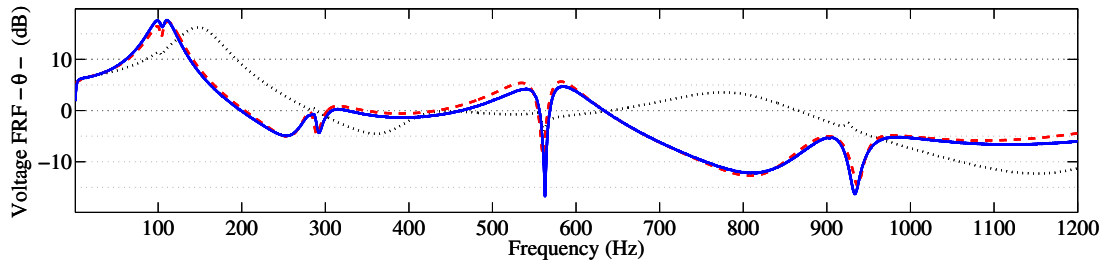


Figure 16. Electrical frequency response functions with measure of the voltage on the 10th pair of patches - (\cdots) for the transfer matrix model with a detuned network, ($---$) for the transfer matrix model with a tuned network, ($—$) for the experiment with a tuned network.

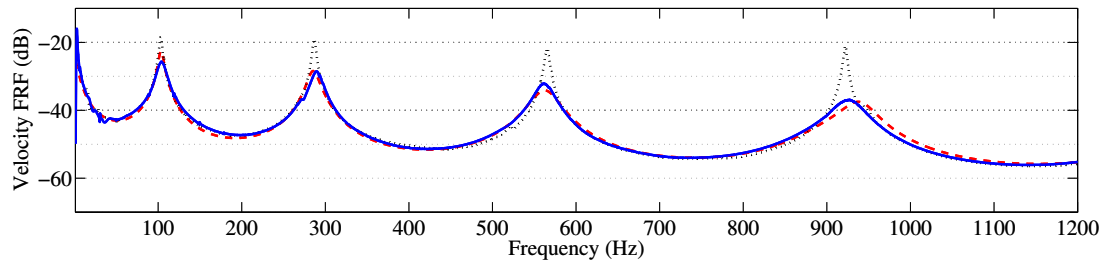


Figure 17. Mechanical frequency response functions - (\cdots) for the experiment with open-circuited patches, ($---$) for the transfer matrix model with a tuned network, ($—$) for the experiment with a tuned network.

considerably reduced by separating the winding of the transformers and using an internal insulation layer. If this choice had been considered before the manufacturing, the results would have been definitely closer to the ones presented in figure 9.

At the end, the comparison between the experiments and the semi-continuous model also validates the theoretical formulation when looking at the mechanical FRF. It can still be remarked that there are slight differences concerning the maximal amplitudes, especially for the first mode that is 3 dB below its theoretical value. This means that an unconsidered damping was added when performing the experiments with the full network. In fact, the mechanical damping coefficient α was determined with open-circuited patches, when all the electrical connectors presented in figure 14 were not yet mounted. The electrical network itself thus increases the purely mechanical damping. This is a point that needs to be improved in future experiments in order to better characterized the vibration reduction only induced by the electromechanical coupling.

5. Conclusions

A multimodal damping strategy is developed in this paper by coupling a beam to its analogue electrical network through piezoelectric patches. A discrete model approximating the mechanical properties of the beam is obtained by performing a finite difference procedure on the Euler-Bernoulli equations. The

corresponding dispersion relation is computed and compared to the one characterizing a continuous beam. The appropriate electrical network is found by applying the direct electromechanical analogy on the discrete model of a beam. A description of the piezoelectric coupling is presented through a linear model including the global properties of the unit cells. The method to determine the global piezoelectric coupling coefficient and the blocked capacitance is given accordingly. Contrary to previous studies that use an electrical homogenization, the network is kept discrete to get closer to real applications with a finite number of piezoelectric patches. Two novel models based on a transfer matrix formulation are presented. Both take into account a discrete electrical network but the first model considers a discrete mechanical medium while the second keeps the continuity of the beam. A modal coupling condition is deduced from the discrete model. It is shown that this condition tunes the electrical resonances to the mechanical ones, which gives a tuned mass effect on several modes together. Then, damping is introduced by considering three different positions for resistors in the network. We observe that the most convenient solution is to include serial resistors after the transformers windings as it can lead to a multimodal damping. To the best of our knowledge, we implemented the first experimental validation of a multimodal damping strategy involving a beam coupled to its discrete electrical analogue. It is also important to notice that the network is completely

passive, without any synthetic components. Finally, it is presented a piezoelectric damping strategy that applies on a wide frequency range. Future works will focus on the extension of the strategy to the control of a plate, which will require a 2D electrical network.

Acknowledgments

This work was funded by the French Ministry of National Education, Higher Education and Research through a three year scholarship for doctoral studies related to structural damping with piezoelectric devices.

- [1] Hagood N W and von Flotow A 1991 *J. Sound Vib.* **146** 243–68.
- [2] Den Hartog J P 1940 *Mechanical vibrations* (New-York: McGraw-Hill)
- [3] Maurini C, Pouget J and Dell’Isola F 2006 *Comput. Struct.* **84** 1438–58.
- [4] Thomas O, Ducarne J and Deü J-F 2012 *Smart Mater. Struct.* **21** 015008.
- [5] Thomas O, Deü J-F and Ducarne J 2009 *Int. J. Numer. Meth. Eng.* **80** 235–68.
- [6] Thorp O, Ruzzene M and Baz A 2001 *Smart Mater. Struct.* **10** 979–989.
- [7] Shengbing C, Jihong W, Gang W, Dianlong Y and Xisen W 2012 *J. Int. Mater. Sys. Struct.* **23** 1613–21.
- [8] Airoidi L and Ruzzene M 2011 *New J. Phys.* **13** 113010.
- [9] Airoidi L and Ruzzene M 2011 *J. Int. Mater. Sys. Struct.* **22** 1567–79
- [10] Wang G, Chen S and Wen J 2011 *Smart Mater. Struct.* **20** 015026.
- [11] Wang G, Wang J, Chen S and Wen J 2011 *Smart Mater. Struct.* **20** 125019.
- [12] Collet M, Cunefare K A and Ichchou M N 2009 *J. Int. Mater. Sys. Struct.* **20** 787–808.
- [13] Beck B S, Cunefare K A, Ruzzene M and Collet M 2011 *J. Int. Mater. Sys. Struct.* **22** 1177–87.
- [14] Mead D M 1996 *J. Sound Vib.* **190** 495–524
- [15] Valis T, von Flotow A and Hagood N W 1994 *J. Sound Vib.* **178** 669–80.
- [16] Vidoli S and Dell’Isola F 2000 *Acta Mech.* **141** 37–50.
- [17] Dell’Isola F, Maurini C and Porfiri M 2004 *Smart Mater. Struct.* **13** 299–308.
- [18] Maurini C, Dell’Isola F and Del Vescovo D 2004 *Mech. Syst. Signal Process.* **18** 1243–71.
- [19] Bisegna P, Caruso G and Maceri F 2006 *J. Sound Vib.* **289** 908–37.
- [20] Batra R C, Dell’Isola F, Vidoli S and Vigilante D 2005 *Int. J. Sol. Struct.* **42** 3115–32.
- [21] Porfiri M, Dell’Isola F and Frattale Mascioli F M 2004 *Int. J. Circ. Theor. Appl.* **32** 167–98.
- [22] Andreaus U, Dell’Isola F and Porfiri M 2004 *J. Vib. Contr.* **10** 625–59.
- [23] Bloch A 1945 *J. Inst. Electr. Eng.* **92** 157–69
- [24] Beranek L L 1954 *Acoustics* (New-York: McGraw-Hill)
- [25] Lossouarn B, Aucejo M, Deü J-F 2015 *Proc. SPIE* 94311A.
- [26] Brillouin L 1946 *Wave propagation in periodic structures* (New-York: McGraw-Hill)
- [27] Lossouarn B, Aucejo M, Deü J-F 2015 *Smart Mater. Struct.* **24** 045018.
- [28] Lu Y and Tang J 2012 *J. Sound Vib.* **331** 3371–85.